

Measuring the Pharmacodynamic Effects of a Novel Hsp90 Inhibitor on HER2/*neu* Expression in Mice Using ^{89}Zr -DFO-Trastuzumab

Jason P. Holland¹, Eloisi Caldas-Lopes², Vadim Divilov¹, Valerie A. Longo³, Tony Taldone², Danuta Zatorska², Gabriela Chiosis², Jason S. Lewis^{1,2*}

1 Radiochemistry Service, Department of Radiology, Memorial Sloan-Kettering Cancer Center, Sloan-Kettering Cancer Center, New York, New York, United States of America, **2** Program in Molecular Pharmacology and Chemistry, Sloan Kettering Institute, Memorial Sloan-Kettering Cancer Center, New York, New York, United States of America, **3** Small-Animal Imaging Core Facility, Memorial Sloan-Kettering Cancer Center, New York, New York, United States of America

Abstract

Background: The positron-emitting radionuclide ^{89}Zr ($t_{1/2} = 3.17$ days) was used to prepare ^{89}Zr -radiolabeled trastuzumab for use as a radiotracer for characterizing HER2/*neu*-positive breast tumors. In addition, pharmacodynamic studies on HER2/*neu* expression levels in response to therapeutic doses of PU-H71 (a specific inhibitor of heat-shock protein 90 [Hsp90]) were conducted.

Methodology/Principal Findings: Trastuzumab was functionalized with desferrioxamine B (DFO) and radiolabeled with [^{89}Zr]Zr-oxalate at room temperature using modified literature methods. ImmunoPET and biodistribution experiments in female, athymic *nu/nu* mice bearing sub-cutaneous BT-474 (HER2/*neu* positive) and/or MDA-MB-468 (HER2/*neu* negative) tumor xenografts were conducted. The change in ^{89}Zr -DFO-trastuzumab tissue uptake in response to high- and low-specific-activity formulations and co-administration of PU-H71 was evaluated by biodistribution studies, Western blot analysis and immunoPET. ^{89}Zr -DFO-trastuzumab radiolabeling proceeded in high radiochemical yield and specific-activity 104.3 ± 2.1 MBq/mg (2.82 ± 0.05 mCi/mg of mAb). *In vitro* assays demonstrated >99% radiochemical purity with an immunoreactive fraction of 0.87 ± 0.07 . *In vivo* biodistribution experiments revealed high specific BT-474 uptake after 24, 48 and 72 h ($64.68 \pm 13.06\%$ ID/g; $71.71 \pm 10.35\%$ ID/g and $85.18 \pm 11.10\%$ ID/g, respectively) with retention of activity for over 120 h. Pre-treatment with PU-H71 was followed by biodistribution studies and immunoPET of ^{89}Zr -DFO-trastuzumab. Expression levels of HER2/*neu* were modulated during the first 24 and 48 h post-administration ($29.75 \pm 4.43\%$ ID/g and $41.42 \pm 3.64\%$ ID/g, respectively). By 72 h radiotracer uptake ($73.64 \pm 12.17\%$ ID/g) and Western blot analysis demonstrated that HER2/*neu* expression recovered to baseline levels.

Conclusions/Significance: The results indicate that ^{89}Zr -DFO-trastuzumab provides quantitative and highly-specific delineation of HER2/*neu* positive tumors, and has potential to be used to measure the efficacy of long-term treatment with Hsp90 inhibitors, like PU-H71, which display extended pharmacodynamic profiles.

Citation: Holland JP, Caldas-Lopes E, Divilov V, Longo VA, Taldone T, et al. (2010) Measuring the Pharmacodynamic Effects of a Novel Hsp90 Inhibitor on HER2/*neu* Expression in Mice Using ^{89}Zr -DFO-Trastuzumab. PLoS ONE 5(1): e8859. doi:10.1371/journal.pone.0008859

Editor: Kenji Hashimoto, Chiba University Center for Forensic Mental Health, Japan

Received: November 2, 2009; **Accepted:** January 5, 2010; **Published:** January 25, 2010

Copyright: © 2010 Holland et al. This is an open-access article distributed under the terms of the Creative Commons Attribution License, which permits unrestricted use, distribution, and reproduction in any medium, provided the original author and source are credited.

Funding: This research was supported by the Geoffrey Beene Cancer Research Center of Memorial Sloan-Kettering Cancer Center (JSL), the Office of Science (BER), U. S. Department of Energy (Award DE-SC0002456, JSL), the U. S. Department of Defense Breast Cancer Research Program (BC085588, GC) and the Susan G. Komen for the Cure (Postdoctoral Fellowship, KG091313, TT). Technical services provided by the MSKCC Small-Animal Imaging Core Facility were supported in part by National Institutes of Health (NIH) grants R24-CA83084, P50-CA086438 and P30-CA08748. The funders had no role in study design, data collection and analysis, decision to publish, or preparation of the manuscript.

Competing Interests: The authors have declared that no competing interests exist.

* E-mail: lewisj2@mskcc.org

Introduction

In the era of molecular medicine, antibody-based agents offer unparalleled potential as platforms for the development of target-specific therapies.[1] Immunoconjugates are monoclonal antibodies (mAbs) or antibody fragments functionalized with cytotoxic and/or diagnostic payloads. Increasing availability of longer-lived positron-emitting radionuclides such as ^{64}Cu , ^{86}Y , ^{89}Zr and ^{124}I , and advances in chelation chemistry, have renewed interest in the use of positron emission tomography with radioimmunoconjugates (immunoPET) as a tool for providing

real-time, quantitative information on physiological response to treatment.[2–5]

Proteins associated with the human epidermal growth-factor receptor kinase (ERBB or HER) signaling network have proved to be valuable targets for diagnostic imaging with radioimmunoconjugates due to their overexpression in various cancers phenotypes. In particular, overexpression of HER2/*neu* (also known as ERBB2) has been found to correlate with increased tumor aggression, metastatic potential, and poor prognosis for disease-free survival in patients with breast, colorectal, ovarian, lung, prostate and salivary gland tumors.[6,7] The ERBB signaling network and the role of

HER2/*neu* in cancer biology has been the subject of several excellent reviews.[7–11]

HER2/*neu* has emerged as a key target for anticancer drugs due to its intrinsic involvement in the phosphatidylinositol-3-kinase-Akt/protein kinase B (PI3K-Akt) and the mitogen-activated protein kinase (MAPK) pathways, both of which suppress apoptosis and promote tumor cell survival, gene transcription, angiogenesis, cellular proliferation, migration, mitosis, and differentiation.[7] Three important classes of anti-HER2/*neu* therapeutics include: mAbs directed against extracellular ligand-binding and dimerization epitopes, tyrosine-kinase (TK) inhibitors and Hsp90 inhibitors. Examples of each class include pertuzumab and trastuzumab (which block dimerization and suppress signaling by binding to extracellular domains II and IV, respectively); the HER2/*neu* TK-inhibitor lapatinib; and Hsp90 inhibitors including geldanamycin derivatives, SNX-5422, NVP-AUY922, BIIB021 and PU-H71.[7,11–18]

Trastuzumab (Herceptin™, Genentech) has been exploited as both a therapeutic agent and radiotracer. Trastuzumab and related mAb-fragments have been radiolabeled with a wide range of radionuclides and quantitative immunoPET imaging has been used to monitor the effect of administering Hsp90 inhibitors on HER2/*neu* expression levels.[19–30] Quantification of changes in HER2/*neu* expression in response to Hsp90 treatment has the potential to facilitate patient-specific dose regimes. For example, studies using ⁶⁴Cu-labeled trastuzumab and ⁶⁸Ga-labeled F(ab')₂-trastuzumab have been reported.[19–21] However, both the ⁶⁴Cu- and ⁶⁸Ga-labeled agents are sub-optimal radiotracers. The comparatively short half-life of ⁶⁴Cu (*t*_{1/2} = 12.7 h) means that the radionuclide has decayed before the intact antibody achieves optimal biodistribution (ca. 4–5 days), and the small size the F(ab')₂ fragments gives poor tumor-to-background tissue contrast ratios.[1,2] In efforts to overcome these limitations in radiotracer design, Orlova *et al.*[28] and Kramer-Marek *et al.*[29] explored the potential of ¹²⁴I- and ¹⁸F-labeled trastuzumab affibodies for measuring HER2/*neu* expression, respectively.

Over recent years, ⁸⁹Zr has emerged as a promising radionuclide for use in immunoPET. In particular, facile methods for radiolabeling intact mAbs with ⁸⁹Zr have been developed from the pioneering work of researchers at the Vrije University Medical Center (Amsterdam, The Netherlands).[30–46] Zirconium-89 has a number of distinct advantages which make it ideal for immunoPET: (i) the half-life of 78.41 h matches closely the extend times required for optimum biodistribution of intact mAbs, (ii) the positron yield of 22.7% is comparable to that of ⁶⁴Cu, ⁸⁶Y and ¹²⁴I which improves counting statistics in PET imaging, (iii) zirconium and its ions are generally inert to biological systems and have no known biological role or function, (iv) cyclotron production of ⁸⁹Zr *via* the (*p,n*) transmutation reaction using a 100% naturally abundant ⁸⁹Y solid target is highly efficient and cost effective,[47] and (v) high purity and high specific-activity ⁸⁹Zr is now available in various chemical forms which are suitable for radiolabeling mAbs. Despite initial concerns over the radiation dosimetry with ⁸⁹Zr which stem from the presence of higher energy γ -rays (*E* γ = 909.2 keV, *I* γ = 99.0%), several clinical studies in Europe have shown that a variety of ⁸⁹Zr-labeled mAbs targeting different tumor types are safe for use in humans.[44–46] Furthermore, these clinical studies demonstrate the benefits of ⁸⁹Zr-labeled mAbs, which in comparison to equivalent mAbs and antibody fragments labeled with other PET radionuclides including ⁶⁴Cu, ⁶⁸Ga, ⁸⁶Y and ¹²⁴I, display higher tumor uptake, lower background tissue accumulation, improved image contrast and more facile delineation of tumors *in vivo*. The use of intact antibodies as the basis for radiotracer development, such as

trastuzumab which is used routinely in the clinic worldwide, also has the advantage of expediting preclinical and clinical translation.

The work presented here describes the production of ⁸⁹Zr-radiolabeled trastuzumab and its ability to identify HER2/*neu* positive tumors *in vivo*. During the course of our investigations, Dijkers *et al.* reported initial studies on ⁸⁹Zr-labeled trastuzumab in the SKOV-3 xenograft model.[30] Our studies further investigate the efficacy of ⁸⁹Zr-DFO-trastuzumab as a radiotracer for immunoPET and include detailed studies using the BT-474 (HER2/*neu* positive) and MDA-MB-468 (HER2/*neu* negative) xenograft models. Our work also complements and extends the methods of Smith-Jones *et al.*[20] which used ⁶⁸Ga-labeled trastuzumab fragments and 17-AAG for measuring pharmacodynamic changes in HER2/*neu* expression *in vivo* to the full antibody with the novel and more potent purine-based Hsp90 inhibitor, PU-H71.[48] Studies include *in vitro* and *in vivo* by Western blot analysis, acute biodistribution studies and immunoPET. The results demonstrate ⁸⁹Zr-radiolabeled trastuzumab has the potential to be used in the clinic as a radiotracer for both localizing and staging of HER2/*neu* positive tumors, and in the long-term measurements of the efficacy of treatment with Hsp90 inhibitors such as PU-H71 and other drugs with extended pharmacodynamic profiles.

Materials and Methods

All chemicals, unless otherwise stated, were purchased from SigmaAldrich (St. Louis, MO) and were used as received. Water (>18.2 M Ω .cm at 25°C, Milli-Q, Millipore, Billerica, MA) was purified by passing through a 10 cm column of chelex resin (Bio-Rad Laboratories, Hercules, CA) at a flow rate <1.0 mL/min. All instruments were calibrated and maintained in accordance with previously reported routine quality-control procedures.[49] Activity measurements were made by using a Capintec CRC-15R Dose Calibrator (Capintec, Ramsey, NJ) with a calibration factor of 465 for ⁸⁹Zr. For accurate quantification of activities, experimental samples were counted for 1 min. on a calibrated Perkin Elmer (Waltham, MA) Automatic Wizard² Gamma Counter by using an energy window of 800–1000 keV for ⁸⁹Zr (909 keV emission). ⁸⁹Zr-radiolabeling reactions were monitored by using silica-gel impregnated glass-fibre instant thin-layer chromatography (ITLC-SG) paper (Pall Corp., East Hills, NY) and analyzed on a radio-TLC plate reader (Bioscan System 200 Imaging Scanner coupled to a Bioscan Autochanger 1000 (Bioscan Inc., Washington, DC), using Win-Scan Radio-TLC software version 2.2). Solvent systems included diethylene triamine pentaacetic acid in water (DTPA, 50 mM, pH 7) and phosphate buffered saline (PBS). Human breast cancer cell lines BT-474 and MDA-MB-468 were obtained from the American Type Culture Collection (ATCC, Manassas, VA) and were grown by serial passage. Full details for all methods are provided in the supporting information (Text S1).

Trastuzumab Conjugation and Radiolabeling

Trastuzumab (Herceptin™, Genentech, South San Francisco, CA) was conjugated to desferrioxamine B (DFO, Calbiochem, Spring Valley, CA) by using procedures modified from those described by Verel *et al.*[36] Full details are provided in the supporting information (Text S1). Briefly, DFO-conjugated trastuzumab (DFO-trastuzumab) was prepared *via* a 6-step procedure involving: the reaction of DFO mesylate with succinic anhydride to give *N*-succinyl-desferrioxamine B; protection of the *tris*-hydroxamate functional groups *via* Fe³⁺ complexation; formation of the tetrafluorophenol (TFP) activated ester; mAb conjugation; removal of the Fe³⁺ *via* transchelation to EDTA;

and purification of DFO-trastuzumab by using size-exclusion chromatography and/or spin-column centrifugal separation.

Zirconium-89 was produced *via* the ⁸⁹Y(*p,n*)⁸⁹Zr transmutation reaction on an EBCO TR19/9 variable-beam energy cyclotron (EbcO Industries Inc., Richmond, British Columbia, Canada) in accordance with previously reported methods.[36,47,50] The [⁸⁹Zr]Zr-oxalate was isolated in high radionuclidic and radiochemical purity (RCP) >99.99%, with a specific-activity of 195–497 MBq/μg, (5.28–13.43 mCi/μg).[47]

⁸⁹Zr-DFO-trastuzumab was prepared by the complexation of [⁸⁹Zr]Zr-oxalate with DFO-trastuzumab. Typical radiolabeling reactions were conducted in accordance with the following procedure. Briefly, [⁸⁹Zr]Zr-oxalate (29.7 MBq, [805 μCi]) in 1.0 M oxalic acid (40 μL) was adjusted to pH 7.7–8.5 with 1.0 M Na₂CO₃(aq.). CAUTION: Acid neutralization releases CO₂(g) and care should be taken to ensure that no radioactivity escapes the microcentrifuge vial. After CO₂(g) evolution ceased, DFO-trastuzumab (50 μL, 5.0 mg/mL [0.25 mg of mAb], in 0.9% sterile saline) was added and the reaction was mixed gently. The reaction was incubated at room temperature for 1–2 h and complexation progress was monitored by ITLC (DTPA, 50 mM, pH 7). After 1 h, high radiolabeling yields were obtained with RCP >78(±4)%. ⁸⁹Zr-DFO-trastuzumab was purified by using either size-exclusion chromatography (Sephadex G-25 M, PD-10 column, >30 kDa, GE Healthcare; dead-volume = 2.5 mL, eluted with 200 μL fractions of 0.9% sterile saline, Figure S1) or spin-column centrifugation (4 mL volume, >30 kDa, Amicon Ultra-4, Millipore, Billerica, MA; washed with 4×3 mL, 0.9% sterile saline). The RCP of the final ⁸⁹Zr-DFO-trastuzumab (>70% radiochemical yield; formulation: pH 5.5–6.0; <500 μL; 0.9% sterile saline) was measured by both radio-ITLC and analytical size-exclusion chromatography (<0.74 MBq [20 μCi], ca. 5–10 μL aliquots) and was found to be >99% in all preparations. In the ITLC experiment ⁸⁹Zr-DFO-trastuzumab and [⁸⁹Zr]Zr-DFO remain at the baseline (*R_f* = 0.0), whereas ⁸⁹Zr⁴⁺(aq.) ions and [⁸⁹Zr]Zr-DTPA elute with the solvent front (*R_f* = 1.0).

Chelate Number

The number of accessible DFO chelates conjugated to trastuzumab was measured by radiometric isotopic dilution assays following a method similar to that described by Anderson *et al* (see supporting information).[51,52] Full details are provided in the supporting information (Text S1).

Immunoreactivity

The immunoreactive fraction of ⁸⁹Zr-DFO-trastuzumab samples was determined by using specific radioactive cellular-binding assays following modified procedures derived from Lindmo *et al*. [53] Briefly, BT-474 or MDA-MB-468 cells were suspended in microcentrifuge tubes at concentrations of 5.0, 4.0, 3.0, 2.5, 2.0, 1.5, and 0.5×10⁶ cells/mL in 500 μL PBS (pH 7.4). Aliquots of ⁸⁹Zr-DFO-trastuzumab (50 μL of a stock solution of <0.37 kBq, [<0.01 mCi] in 10 mL of 1% bovine serum albumin [BSA]; 2 kBq [0.05 μCi], 0.02 μg of mAb) were added to each tube (*n* = 3; final volume: 550 μL) and the samples incubated on an orbital mixer for 60 min. at room temperature. Cells were then pelleted by centrifugation (600G for 2 min.), resuspended and washed twice with ice-cold PBS before removing the supernatant and counting the ⁸⁹Zr-activity associated with the cell pellet. The count data were background corrected and compared with the total number of counts in control samples. Competitive inhibition (blocking) studies were conducted by using the same procedure but with the addition of non-radiolabeled trastuzumab (50 μL, 2 mg/mL in 1% BSA, [>5000-fold excess mAb; 100 μg]) to the ⁸⁹Zr-DFO-trastuzumab solutions.

Immunoreactive fractions were determined by linear regression analysis of a plot of (total/bound) activity *versus* (1/[normalized cell concentration]), and calculated as 1/*γ*-intercept. Full details are provided in the supporting information (Text S1).

Stability Studies

The stability of ⁸⁹Zr-DFO-trastuzumab with respect to radiochemical purity, loss of radioactivity from the mAb and change in immunoreactivity was investigated *in vitro* by incubation in solutions of 0.9% saline, DTPA (50 mM, pH 7) and human serum for 7 days at 37°C. The radiochemical purity and degree of transchelation to DTPA was determined by radio-ITLC and *γ*-counting, and the immunoreactive fraction was measured by the cellular-binding assay (*vide supra*).

Xenograft Models

All animal experiments were conducted in compliance with the guidelines of the Institutional Animal Care and Use Committee (IACUC) of MSKCC. Female athymic *nu/nu* mice (NCRNU-M, 20–22 g, 6–8 weeks old) were obtained from Taconic Farms Inc. (Hudson, NY), and were acclimated to the MSKCC vivarium for 1 week prior to implanting tumors. Mice were provided with food and water *ad libitum*. Tumors were induced on a shoulder by subcutaneous (s.c.) injection of 5.0–10.0 (×10⁶) cells in a 200 μL cell suspension of a 1:1v/v mixture of media with reconstituted basement membrane (BD Matrigel™, Collaborative Biomedical Products Inc., Bedford, MA).[54] For animals bearing two tumors used in the immunoPET studies, BT-474 and MDA-MB-468 cells were implanted s.c. on the left and right shoulder/flank, respectively. Palpable tumors developed after a period of 14–18 days and the tumor volume (V/mm³) was estimated by external vernier caliper measurements (Full details are provided in the supporting information (Text S1)).[55]

Acute Biodistribution Studies

Acute *in vivo* biodistribution studies were conducted to evaluate the uptake of ⁸⁹Zr-DFO-trastuzumab in mice bearing s.c. BT-474 tumors (90–170 mm³). Mice were randomized before the study and were warmed gently with a heat lamp 5 min. before administering ⁸⁹Zr-DFO-trastuzumab (0.55–0.74 MBq, [15–20 μCi], 5–7 μg of mAb, in 200 μL 0.9% sterile saline) *via* intravenous (i.v.) tail-vein injection (*t* = 0 h). Animals (*n* = 3–8, per group) were euthanized by CO₂(g) asphyxiation at 1, 12, 24, 48, 72 and 120 h post-injection and 12 organs (including the tumor) were removed, rinsed in water, dried in air for 5 min., weighed and counted in a gamma-counter for ⁸⁹Zr-activity. The mass of ⁸⁹Zr-DFO-trastuzumab formulation injected into each animal was measured and used to determine the total number of counts (counts per minute, [c.p.m.]) by comparison to a standard syringe containing and independently measured activity and mass. Count data were background and decay-corrected to the time of injection and the percent injected dose per gram (%ID/g) for each tissue sample calculated by normalization to the total activity injected.

The effects of pre-administering PU-H71 (intraperitoneal (i.p.), 75 mg/kg, 200 μL of PU-H71-hydrochloride dissolved in 10 mM phosphate buffer [PB]) 4 h prior to i.v. injection of ⁸⁹Zr-DFO-trastuzumab, were also investigated by acute biodistribution studies at 12, 24, 48 and 72 h.

Competitive inhibition studies were also performed to investigate the specificity of ⁸⁹Zr-DFO-trastuzumab for HER2/*neu*. Non-radiolabeled trastuzumab (10 mg/kg solution in 0.9% sterile saline, 0.2 mg/mouse) was added to the ⁸⁹Zr-DFO-trastuzumab formulation to reduce the specific-activity (30–40-fold decrease:

2.60–3.65 MBq/mg [0.07–0.1 mCi/mg]) and biodistribution studies were performed at 24 h post-i.v. administration.

Pharmacodynamic Studies

Changes in the expression levels of HER2/*neu* in response to Hsp90 inhibition were investigated by *in vivo* pharmacodynamic (PD) studies. Prior to BT-474 cell inoculation, mice were implanted s.c. with 0.72 mg sustained release 17 β -estradiol pellets by using a 10 g trocar. Tumors were established as described above and were allowed to grow to 6–8 mm in diameter (120–270 mm³) before commencing treatment. Mice ($n = 2$, per group) bearing s.c. BT-474 tumors were administered PU-H71 (as the hydrochloride salt, i.p., 75 mg/kg, 200 μ L, 10 mM PB). Animals were euthanized by CO₂(g) asphyxiation at 12, 24, 48, 72 and 96 h post-i.p. administration of PU-H71 and tumors were collected. For protein analysis, tumors were homogenized in SDS lysis buffer (50 mM Tris, pH 7.4, 150 mM NaCl, and 1% Nonidet P-40) and subjected to Western blot analysis (*vide infra*).

Western Blots

BT-474 cells were grown to 60–70% confluence and treated with either PU-H71 (in 10 mM PB) at various concentrations or DMSO for the specified time. Lysates were prepared by using 50 mM Tris, pH 7.4, 150 mM NaCl, and 1% Nonidet P-40 lysis buffer. Protein concentrations were determined by using the bicinchoninic acid (BCA) Protein Assay kit (Pierce, Rockford, IL) in accordance with the manufacturer's protocol. Protein lysates (20–100 μ g) were resolved electrophoretically by SDS-PAGE, transferred to nitrocellulose membrane, and then probed with the specified primary antibodies: anti-HER2 from rabbit (1:250, 280004; Zymed Laboratories Inc., South San Francisco, CA); anti-PARP (p85 fragment) from rabbit (1:250, G7341; Promega, Madison, WI); anti-phospho-Akt (Ser 473) from rabbit (1:500, 9271S; Cell Signaling); anti-Akt from rabbit (1:500, 9272; Cell Signaling Technology Inc., Danvers, MA); anti-Hsp70 from mouse (1:500, SPA-810; Stressgen, Ann Arbor, MI); anti-Hsp90 from mouse (1:500, SPA-830; Stressgen); and anti-Raf-1 from rabbit (1:300, sc-133; Santa Cruz Biotechnology Inc., Santa Cruz, CA). Membranes were then incubated with a 1:5,000 dilution of a corresponding peroxidase-conjugated secondary antibody. Equal loading of the protein samples was confirmed by parallel Western blots for β -actin (1:5,000, ab8227–50; Abcam Inc., Cambridge, MA). Detection was performed by using the ECL-Enhanced Chemiluminescence Detection System (Amersham Biosciences, Fairfield, CT) according to the manufacturer's instructions. Blots were visualized by autoradiography.[48] Gels were scanned using Adobe Photoshop 7.0.1 and semi-quantitative densitometric analysis was performed by using Un-Scan-It software.

Small-Animal ImmunoPET Imaging

PET imaging experiments were conducted on a microPET Focus 120 rodent scanner (Concorde Microsystems).[56] Mice were administered ⁸⁹Zr-DFO-trastuzumab formulations (8.50–9.25 MBq, [230–250 μ Ci], 80–90 μ g of mAb, in 200 μ L 0.9% sterile saline for injection) *via* tail-vein injection. The effects of pre-administering PU-H71 (i.p., 75 mg/kg, 200 μ L of PU-H71-hydrochloride dissolved in 10 mM phosphate buffer [PB]) or vehicle-control, 4 h prior to i.v. injection of ⁸⁹Zr-DFO-trastuzumab, were also investigated by immunoPET. Approximately 5 minutes prior to recording PET images, mice were anesthetized by inhalation of 2% isoflurane (Baxter Healthcare, Deerfield, IL)/oxygen gas mixture and placed on the scanner bed; anesthesia was maintained using 1% isoflurane/oxygen gas mixture. PET data were recorded at various time-points between 1–120 h. List-mode

data were acquired for 10–30 min. using a γ -ray energy window of 350–750 keV, and a coincidence timing window of 6 ns. Images were analyzed by using ASIPro VMTM software (Concorde Microsystems). Full experimental details are presented in the supporting information. Full details are provided in the supporting information (Text S1).

Statistical Analysis

Data were analyzed by the unpaired, two-tailed Student's *t*-test. Differences at the 95% confidence level ($P < 0.05$) were considered to be statistically significant.

Results and Discussion

During the course of our investigations, Dijkers *et al.* reported initial studies using ⁸⁹Zr-labeled trastuzumab in SKOV-3 (HER2/*neu* positive) xenograft models.[30] In these studies we have extended the use ⁸⁹Zr-DFO-trastuzumab to investigate uptake in the BT-474 (HER2/*neu* positive) and MDA-MB-468 (HER2/*neu* negative) xenograft models. We have also explored the potential of ⁸⁹Zr-DFO-trastuzumab to be used as a non-invasive radiotracer for qualitative and quantitative delineation of the efficacy of Hsp90 inhibitor treatment (namely PU-H71) on HER2/*neu* expression levels *in vivo*.

⁸⁹Zr-DFO-Trastuzumab Was Produced in High Yield and Specific-Activity

Trastuzumab was functionalized with the hexadentate, trihydroxamate chelate, desferrioxamine B (DFO) by using bioconjugation methods modified from the pioneering work of Verel *et al.*[36] Previous studies have shown that although DTPA can be used for chelation and radiolabeling of mAbs with ⁸⁹Zr⁴⁺ ions, demetalation occurs *in vivo* and at present DFO remains the chelate of choice.[31,33,47] Despite the multi-step functionalization methods involving protection/deprotection using Fe³⁺ ions the conjugation and purification chemistry was found to proceed in moderate-to-high yield (60–78%) with high purity. Radiolabeling of sterile DFO-trastuzumab with either [⁸⁹Zr]Zr-oxalate or [⁸⁹Zr]Zr-chloride was achieved at room temperature in alkaline solutions (pH 7.7–8.5) with crude radiochemical yields (>95%, $n = 15$). Facile purification of ⁸⁹Zr-DFO-trastuzumab from small-molecule radiolabeled impurities can be achieved by using either size-exclusion chromatography or spin-column centrifugation. The final radiochemical yield of purified ⁸⁹Zr-DFO-trastuzumab was >70% and the product was formulated in either PBS or 0.9% sterile saline with RCP >99% ($n = 12$) and a specific-activity of 104.3 \pm 2.1 MBq/mg (2.82 \pm 0.05 mCi/mg) of mAb. The specific-activity obtained in our studies compares favorably with the previously reported specific-activity of 67.2 \pm 2.4 MBq/mg (1.82 \pm 0.07 mCi/mg).[30] Isotopic dilution assays revealed an average of 6.8 \pm 0.8 accessible chelates per mAb.

⁸⁹Zr-DFO-Trastuzumab Is Stable and Immunoreactive *In Vitro*

Incubation of ⁸⁹Zr-DFO-trastuzumab in either 0.9% sterile saline or human serum for 7 days at 37°C revealed <2% decrease in RCP (*via* demetalation) with a \sim 27% decrease in immunoreactive fraction (0.60 \pm 0.02). In contrast, experiments conducted in DTPA (50 mM, pH 7) showed a 55 \pm 2% decrease in RCP after 7 days. DTPA represents a particularly strong ligand challenge and overall these results are consistent with other reports which indicate that ⁸⁹Zr-DFO-mAbs display high kinetic stability and are suitable for further *in vivo* studies.[30,35,40,43–45]

The immunoreactive fraction of the ⁸⁹Zr-DFO-trastuzumab formulations was measured by specific *in vitro* cellular association assays using BT-474, HER2/*neu* positive cells prior to each *in vivo* experiment (Figure 1).[53] The average immunoreactive fraction of ⁸⁹Zr-DFO-trastuzumab was found to be 0.87±0.07 (n=18). Control experiments (n=3) using the HER2/*neu* negative MDA-MB-468 cell line or BT-474 cells with low specific-activity formulations (0.37±0.1 MBq/mg [10.2±0.2 µCi/mg]) in which a >5000-fold excess of non-radiolabeled trastuzumab was added to the reactions showed no binding and demonstrated the specificity of ⁸⁹Zr-DFO-trastuzumab for HER2/*neu* expressing cells (Figures S2A and S2B).

In Vitro Pharmacodynamic Studies Demonstrate the Effects of PU-H71 on HER2/*neu* Expression

In HER2/*neu* positive tumors, Hsp90 has been shown to regulate the expression levels of a variety of onco-proteins including HER2/*neu*. [18,57] *In vitro* Western blot studies showed that treatment of BT-474 cells with varying concentrations of PU-H71 (1–0.01 µM, Figure S3) for 24 h led to changes in expression levels of proteins associated with the ERBB signaling cascade (Figure 2). In each case, expression levels of the Hsp90-independent protein β-actin, was used as a protein loading control. Consistent with the Hsp90-mediated mechanism of action, PU-H71 treatment at concentrations ≥0.25 µM, decreased expression levels of Hsp90 client onco-proteins including HER2/*neu*, Akt and RAF1, compared to DMSO-treated controls. Degradation of Akt and phosphorylated Akt (P-Akt) leads to inactivation of cell survival pathways and the observed concomitant increase in levels of cleaved poly-(ADP-ribose) polymerase (cPARP) is indicative of apoptosis. Decreased expression levels of RAF1 demonstrate that PU-H71 inhibition of Hsp90 also inhibits the MAPK signaling pathway, consequently suppressing the transcription of genes associated with cell survival, angiogenesis, proliferation, migration, mitosis, and differentiation. Experiments also revealed that expression levels of Hsp90 remained constant with varying PU-H71 concentrations but Hsp70 levels increased in response to Hsp90 inhibition at concentrations of approximately 0.1–0.25 µM.

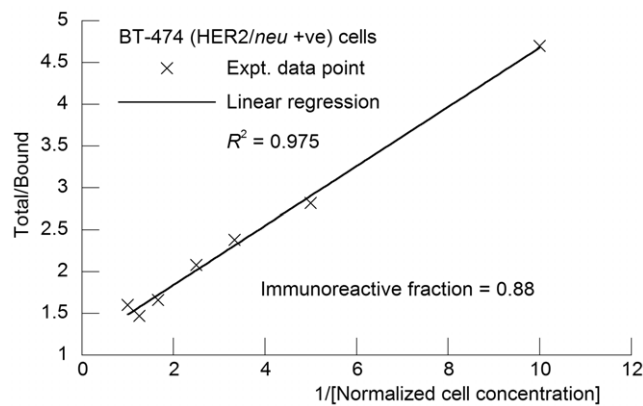


Figure 1. Plot of the (total/bound) activity versus 1/[normalized cell concentration], used to calculate the immunoreactivity fraction of ⁸⁹Zr-DFO-trastuzumab in BT-474 (HER2/*neu* positive) cells by extrapolation to infinite antigen excess (1/y-intercept).
doi:10.1371/journal.pone.0008859.g001

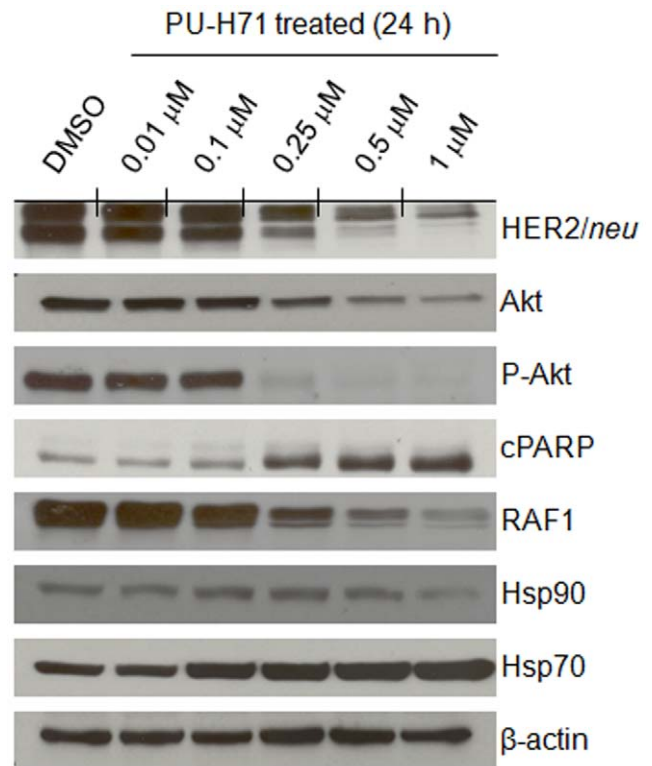


Figure 2. *In vitro* Western blots showing the change in protein expression levels in response to treatment with PU-H71 at 0.01–1 µM concentrations. DMSO vehicle treated experiments and β-actin are include as controls. Proteins investigated include: HER2/*neu*; Akt; phosphorylated Akt (P-Akt); the apoptosis marker, cleaved poly (ADP-ribose) polymerase (cPARP); RAF1; Hsp90; Hsp70; and β-actin as a protein loading control.
doi:10.1371/journal.pone.0008859.g002

Biodistribution Studies Show Specific Uptake of ⁸⁹Zr-DFO-Trastuzumab in BT-474 Tumors

The ability of ⁸⁹Zr-DFO-trastuzumab to target HER2/*neu* receptors *in vivo* was initially assessed by conducting acute biodistribution studies in BT-474 tumor-bearing mice at 1, 12, 24, 48, 72 and 120 h post-i.v. administration (Tables 1 and S1, and Figure 3). The data reveal that high tumor uptake is observed 24 h post-injection (64.68±13.06%ID/g) with ⁸⁹Zr accumulation in the tumors reaching a peak between 48 and 72 h. Retention of ⁸⁹Zr was observed for over 120 h (75.54±13.47%ID/g) with only a small decrease (9.64%ID/g, [P=0.28]) in the mean uptake compared to that at 72 h.

Competitive inhibition studies using low specific-activity formulations (30–40-fold decrease: 2.60–3.65 MBq/mg [0.07–0.1 mCi/mg]) revealed only 13.50±4.84%ID/g tumor uptake at 24 h post-injection; an approximate 5-fold decrease (P<0.00001) versus high specific-activity formulations (Figure 3A). These experiments concur with the *in vitro* data and demonstrate the specificity of ⁸⁹Zr-DFO-trastuzumab for the HER2/*neu* antigen *in vivo*.

The pharmacodynamic effects of administering PU-H71 on ⁸⁹Zr-DFO-trastuzumab uptake in BT-474 tumor-bearing mice were also investigated by using acute biodistribution studies (Table 1 and S1, and Figure 3B) and Western blot analysis of tissue samples (Figure 4). Animals were treated with a single dose of PU-H71 4 h prior to i.v. injection of ⁸⁹Zr-DFO-trastuzumab (t=0 h) and biodistribution studies were conducted at 12, 24, 48 and 72 h. The biodistribution data show that at 24 and 48 h post-injection,

Table 1. Biodistribution data of ⁸⁹Zr-DFO-trastuzumab versus time/h, administered by i.v. tail-vein injection to female, athymic *nu/nu* mice bearing s.c. BT-474 tumors (90–150 mm³).^{a,b}

⁸⁹ Zr-DFO-trastuzumab (5–7 µg mAb)						
Organ	1 h (n=5)	12 h (n=4)	24 h (n=8)	48 h (n=3)	72 h (n=8)	120 h (n=4)
Blood	45.29±9.33	23.70±3.28	18.68±3.12	18.83±3.35	17.23±5.06	11.05±6.98
Tumor	7.35±3.22	23.80±3.37	64.68±13.06	71.71±10.35	85.18±11.10	75.54±13.47
Heart	12.61±3.38	8.22±3.46	5.05±0.90	6.58±1.98	4.75±1.62	3.25±1.35
Lung	18.09±3.48	14.50±2.79	12.36±1.87	13.02±2.72	12.76±3.78	7.11±4.07
Liver	21.18±4.97	8.44±0.98	10.10±1.02	9.96±1.99	9.48±1.13	10.55±2.78
Spleen	22.50±8.89	7.85±1.28	10.92±2.29	6.34±1.69	10.82±3.80	10.85±3.18
Kidney	12.02±2.72	8.43±0.63	7.28±0.66	7.59±1.21	7.75±1.23	6.48±1.67
Muscle	0.68±0.08	1.36±0.38	1.22±0.18	1.12±0.26	1.25±0.40	1.03±0.42
Bone	5.64±0.90	1.93±0.71	3.67±1.71	1.68±0.47	4.79±0.65	6.86±3.02
Tumor/Blood	0.17±0.09	1.06±0.23	3.50±0.78	3.91±1.04	5.18±1.90	5.68±2.13
Tumor/Heart	0.64±0.32	3.52±2.03	12.94±2.75	11.71±4.44	19.59±6.30	20.26±5.81
Tumor/Lung	0.44±0.27	1.80±0.72	5.25±0.90	5.75±1.90	7.09±2.47	9.27±3.62
Tumor/Liver	0.36±0.14	2.86±0.74	6.39±1.11	7.37±1.54	9.44±1.98	8.20±1.54
Tumor/Spleen	0.33±0.09	2.93±0.88	5.99±1.04	11.84±3.25	9.21±2.59	8.06±1.48
Tumor/Kidney	0.66±0.36	2.95±0.62	8.83±1.36	9.65±2.33	10.98±1.59	10.54±2.40
Tumor/Muscle	11.30±5.80	18.34±9.95	54.27±5.07	67.80±4.51	75.81±6.63	67.67±5.94
Tumor/Bone	1.32±0.55	10.01±1.50	9.63±6.73	45.55±16.54	18.41±4.90	14.21±2.79
Block (200 µg mAb)		PU-H71 treated (5–7 µg mAb)				
Organ	24 h (n=4)	12 h (n=5)	24 h (n=5)	48 h (n=4)	72 h (n=5)	
Blood	47.02±12.72	24.89±1.54	20.79±7.20	21.59±3.67	22.63±6.88	
Tumor	13.50±4.84	14.55±2.75	29.75±4.43	41.42±3.64	73.64±12.17	
Heart	12.58±3.95	8.36±1.67	5.01±0.63	4.48±1.51	5.69±0.45	
Lung	25.28±7.34	15.64±1.85	12.84±5.39	13.55±3.82	13.16±3.45	
Liver	28.37±5.49	9.74±1.20	10.02±1.80	11.46±1.52	12.89±1.04	
Spleen	33.22±8.01	9.94±2.01	11.20±2.52	10.15±2.44	12.66±4.92	
Kidney	12.33±2.39	8.89±1.00	8.46±1.81	7.64±1.07	9.55±1.59	
Muscle	0.87±0.17	1.18±0.15	1.27±0.23	0.97±0.28	1.55±0.40	
Bone	7.79±2.39	2.66±0.99	5.09±2.32	2.23±0.47	5.27±1.48	
Tumor/Blood	0.33±0.20	0.55±0.09	1.53±0.51	1.96±0.23	3.36±0.52	
Tumor/Heart	1.28±0.89	1.76±0.82	6.22±1.56	8.16±1.09	12.89±1.16	
Tumor/Lung	0.67±0.23	0.89±0.06	2.74±1.28	3.55±0.64	5.70±0.61	
Tumor/Liver	0.48±0.30	1.43±0.05	3.27±0.77	3.79±0.39	5.78±1.36	
Tumor/Spleen	0.50±0.20	1.36±0.02	2.82±0.85	4.68±0.18	6.54±2.81	
Tumor/Kidney	1.17±0.56	1.49±0.30	3.54±0.44	5.16±0.13	7.71±0.28	
Tumor/Muscle	16.61±7.61	12.54±1.35	24.90±2.74	36.93±1.47	48.47±5.39	
Tumor/Bone	1.90±1.03	4.64±0.92	7.86±3.86	21.17±5.14	14.98±5.44	

^aComplete biodistribution data are presented in the supporting information (Table S1).

^bThe data are expressed as the mean %ID/g ± one standard deviation (S.D.).

doi:10.1371/journal.pone.0008859.t001

tumor uptake in PU-H71-treated mice reached 29.75±4.43%ID/g and 41.42±3.64%ID/g, respectively. Thus, in comparison with control experiments, PU-H71 inhibition of Hsp90 and degradation of HER2/*neu* results in approximately 50% decrease in ⁸⁹Zr-DFO-trastuzumab tumor uptake at 24 and 72 h (Table S2; Control-to-PU-H71-treated %ID/g ratios of 2.17 [*P*=0.0001] and 1.73 [*P*=0.026], respectively). By 72 h post-administration, ⁸⁹Zr-DFO-trastuzumab tumor uptake in PU-H71-treated mice (73.64±12.17%ID/g) returned to the same levels as observed in

the control experiments (85.18±11.10%ID/g, [*P*=0.244]). Importantly, ⁸⁹Zr-DFO-trastuzumab uptake in all background tissues remained the same in control and PU-H71 treated animals. This observation demonstrates the specificity of PU-H71 for HER2/*neu* over-expressing BT-474 tumors.

The ⁸⁹Zr-DFO-trastuzumab biodistribution data suggest that a single-dose of PU-H71 induces a sustained effect in terms of HER2/*neu* and other client oncoprotein degradation for at least 48 h post-administration. This observation was confirmed by

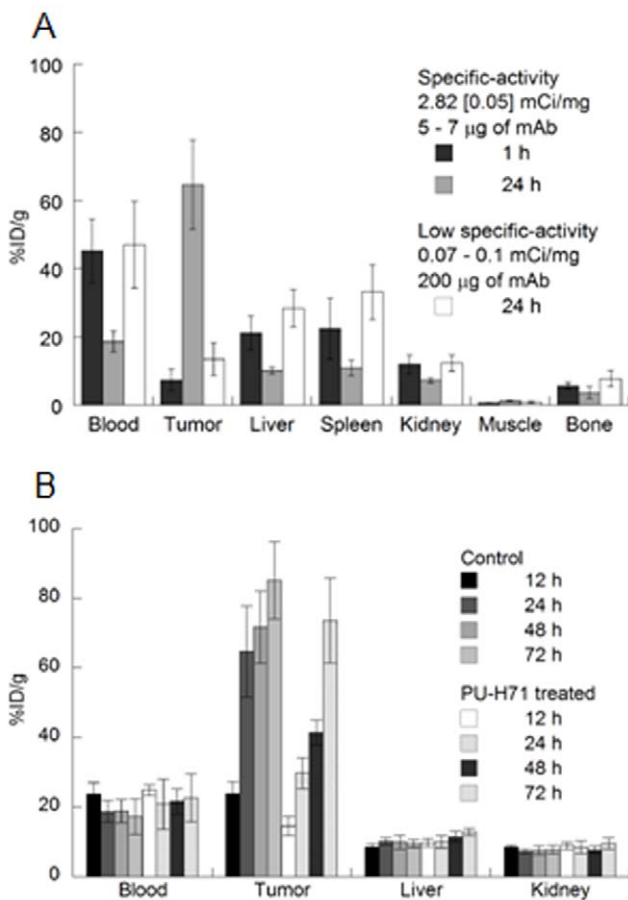


Figure 3. Bar charts showing selected tissue biodistribution data (%ID/g) for (A) uptake of high and low specific-activity formulations of ⁸⁹Zr-DFO-trastuzumab in BT-474 tumor-bearing mice, and (B) ⁸⁹Zr-DFO-trastuzumab uptake in control (vehicle-treated) and PU-H71 treated animals at 12, 24, 48 and 72 h post-i.v. administration of ⁸⁹Zr-DFO-trastuzumab (0.55–0.74 MBq, 5–7 µg of mAb, in 200 µL 0.9% sterile saline).
doi:10.1371/journal.pone.0008859.g003

conducting Western blot analysis for HER2/*neu* expression in homogenized tumor tissue samples obtained at 0, 12, 24, 48, 72 and 96 h post-i.p. administration of PU-H71 in BT-474 tumor-bearing mice (Figures 4A and B). As with the *in vitro* experiments, PU-H71 was found to inhibit Hsp90 as indicated by the specific tumor fingerprints which showed increased Hsp70 expression, degradation of P-Akt and high levels of cPARP between 24 and 72 h. The data confirm that PU-H71 degrades HER2/*neu* levels to ~20% of initial levels for up to 48 h. HER2/*neu* expression was found to return to baseline levels by 72 h. The recovery of HER2/*neu* expression between 48 and 72 h is consistent with the increase in ⁸⁹Zr-DFO-trastuzumab uptake observed in the biodistribution studies.

ImmunoPET Studies Demonstrate the Use of ⁸⁹Zr-DFO-Trastuzumab as a Radiotracer

ImmunoPET images of ⁸⁹Zr-DFO-trastuzumab recorded in BT-474 and MDA-MB-468 tumor-bearing mice between 1 to 120 h are presented in Figures 5A and B, respectively. Radiotracer uptake in BT-474 tumors was observed in <5 h post-injection of ⁸⁹Zr-DFO-trastuzumab and high tumor-to-muscle (T/M) ratios (calculated by using both region-of-interest mean and maximum

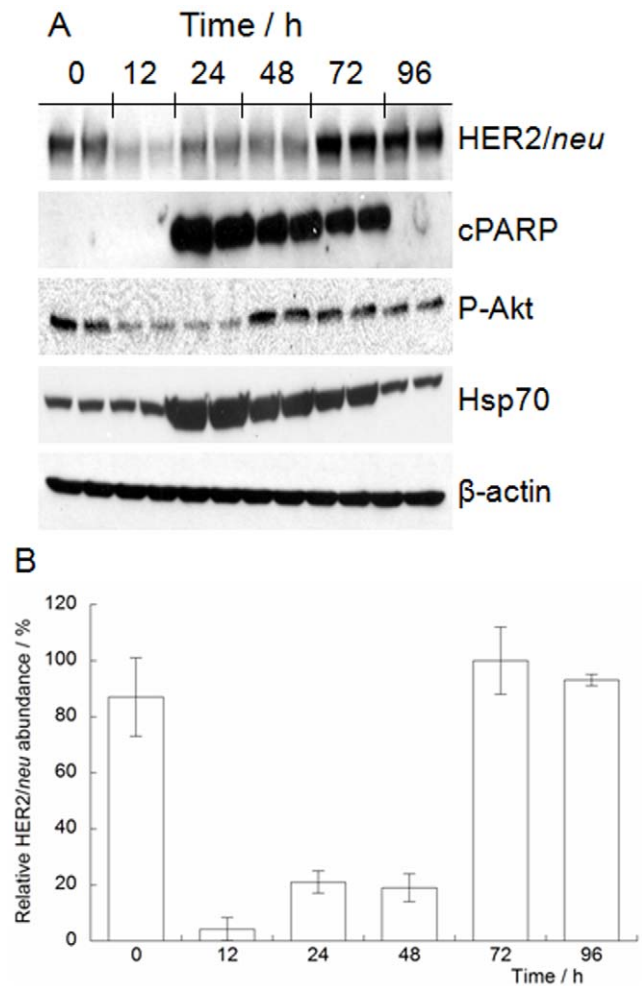


Figure 4. Pharmacodynamic studies on protein expression levels in BT-474 tumor tissue samples obtained at 12, 24, 48, 72 and 96 h after PU-H71 treatment.
doi:10.1371/journal.pone.0008859.g004

%ID/g values from the PET images; Figure 6 and Table S3) were observed. At 5 h post-injection mean and maximum T/M ratios for radiotracer uptake in BT-474 tumor-bearing mice were found to be 7.87 and 11.90, respectively. In contrast, low ⁸⁹Zr-DFO-trastuzumab accumulation in HER2/*neu* negative MDA-MB-468 tumors (mean and maximum T/M ratios of 2.26 and 4.15, respectively) was found to occur in accordance with the “enhanced permeation and retention” (EPR) mechanism.[58]

Quantification of the immunoPET images showed that at 48 and 72 h time points, the absolute uptake of ⁸⁹Zr-DFO-trastuzumab was around 16.0%ID/g in BT-474 tumors and 4.5%ID/g in MDA-MB-468 tumors (Figure 6). These data show that ⁸⁹Zr-DFO-trastuzumab immunoPET imaging provides very high tumor-to-background tissue (T/B) ratios. Although the models are not identical which prevents direct comparison, the high contrast observed in the immunoPET images with ⁸⁹Zr-DFO-trastuzumab compare favorably with those obtained using other mAb and mAb-fragments labeled with ⁶⁴Cu, ⁶⁸Ga, ⁸⁶Y, ^{99m}Tc, ¹¹¹In or ¹²⁴I. [19–30] Although the immunoPET images demonstrated very high contrast for radiotracer uptake in BT-474 tumors, quantitative analysis suggests that ⁸⁹Zr-DFO-trastuzumab is approximately 5-fold lower than was observed in the biodistribution experiments. This discrepancy is explained by

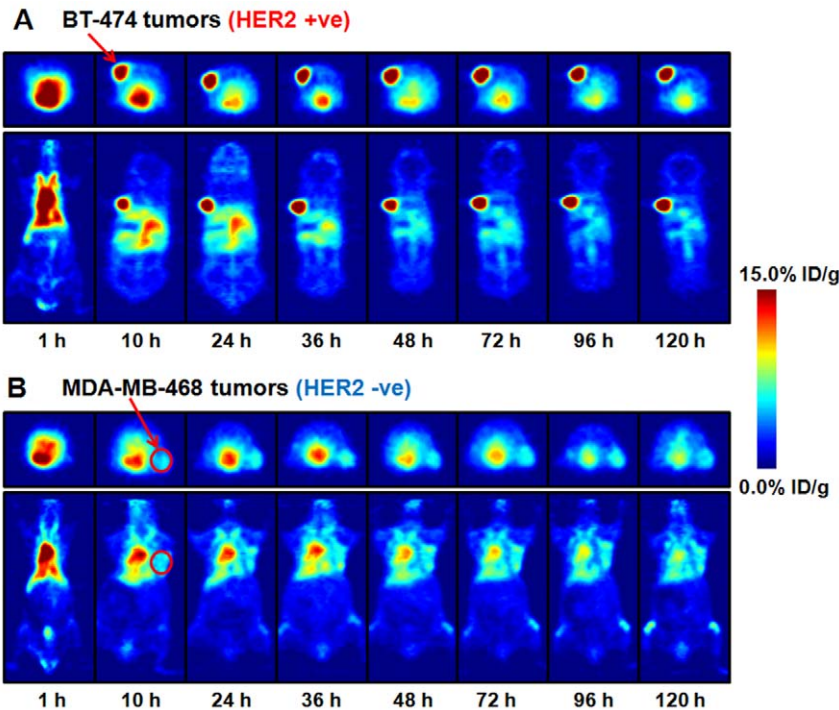


Figure 5. ImmunoPET images of ⁸⁹Zr-DFO-trastuzumab (8.50–9.25 MBq, 80–90 μg of mAb, in 200 μL 0.9% sterile saline) recorded in (A) BT-474 (left shoulder) and (B) MDA-MB-468 (right flank) tumor-bearing mice between 1–120 h post-injection. The transverse (top) and coronal (bottom) planar images intersect the center of the tumors. doi:10.1371/journal.pone.0008859.g005

considering the difference in the amount of mAb administered between the two experiments. For the immunoPET experiments a total of 80–90 μg of trastuzumab was administered, whereas in the biodistribution assays only 5–7 μg was used. The use of different total doses of trastuzumab is unavoidable given the limitations in sensitivity of small-animal PET detection which requires larger amounts of administered activity than simple biodistribution experiments. In humans undergoing trastuzumab therapy, the mAb is administered at concentrations >5 mg/kg.[59] Based on the human values, a therapeutic dose of trastuzumab in a typical 20–25 g mouse, corresponds to 100–125 μg of mAb. Consequent-

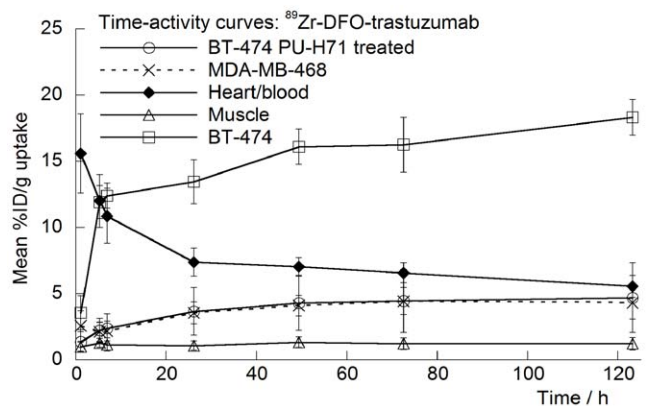


Figure 6. Time-activity curves derived by region-of-interest analysis of the immunoPET images showing the mean %ID/g tissue uptake versus time/h, for control and PU-H71-treated mice bearing both BT-474 and MDA-MB-468 tumors. doi:10.1371/journal.pone.0008859.g006

ly, the specific-activity of ⁸⁹Zr-DFO-trastuzumab becomes a factor in determining the precise correlation between the uptake values obtained from the biodistribution and quantitative immunoPET images. In other words, at the specific-activity obtained, the amount of mAb administered in the immunoPET experiments causes approximately 80% competitive binding (blocking) of available HER2/neu antigens with non-radiolabeled trastuzumab. Importantly, previous studies in our laboratory using the Focus 120 microPET and “non-saturating” PET radiotracers have demonstrated close agreement between imaging and biodistribution-derived activity concentrations.

ImmunoPET studies were also used to visualize and quantify the pharmacodynamic effects of PU-H71 treatment in dual tumor-bearing mice. The immunoPET images (Figure 7) and time-activity curves (TACs; Figure 6) show that in PU-H71 treated mice, no difference was observed in either the mean or maximum T/M ratios between BT-474 and MDA-MB-468 tumors. For example, 24 h after administering ⁸⁹Zr-DFO-trastuzumab mean T/M ratios in PU-H71-treated mice were measured as 2.57 and 3.00 in BT-474 and MDA-MB-468 tumors, respectively (Figure 7 and Table S3).

In contrast, large differences were observed in the measured T/M ratios between BT-474 (T/M = 7.63) and MDA-MB-468 (T/M = 2.82) tumors in vehicle-treated mice. At longer time points, mean T/M ratios for BT-474 tumors in vehicle-treated mice remained constant at 48 h (7.85) but decreased slightly by 72 h (6.71) and 120 h (6.77).

The approximate 3-fold decrease in BT-474 T/M ratios between the vehicle-treated and PU-H71 treated mice is consistent with the decrease in HER2/neu expression levels observed by *in vivo* Western blots (Figure 4). Furthermore, the slight decrease in tumor uptake between 72 and 120 h is consistent with the 9.6%ID/g decrease in BT-474 tumor uptake observed from the

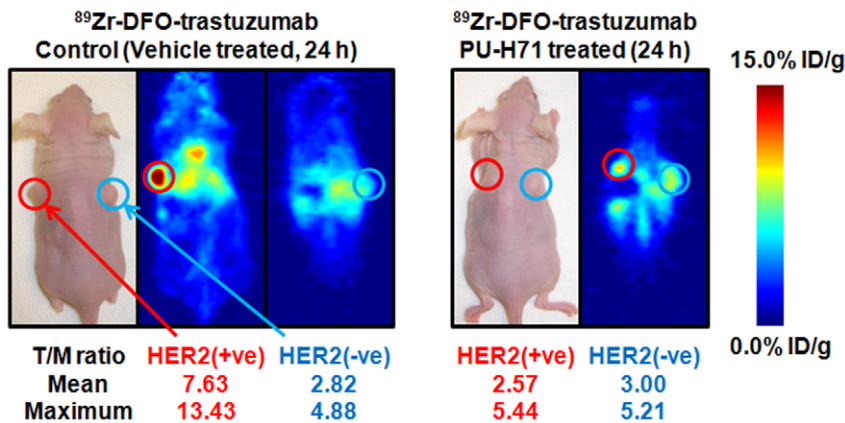


Figure 7. Coronal immunoPET images of control (left) and PU-H71 (right) treated mice bearing s.c. BT-474 and MDA-MB-468 tumors recorded at 24 h post-i.v. administration of ⁸⁹Zr-DFO-trastuzumab. Mean and maximum T/M ratios obtained from VOI analysis are presented (Table S3). For the control animal, the two coronal PET slices lie through the center of the HER2/*neu* positive and negative tumors. doi:10.1371/journal.pone.0008859.g007

biodistribution studies. This decreased tumor uptake at longer time points is potentially indicative of a slow rate of metabolism and excretion of ⁸⁹Zr⁴⁺ after internalization of HER2/*neu*-bound ⁸⁹Zr-DFO-trastuzumab (Figures S4 and S5, and Table S4).

At late time points, the biodistribution data for ⁸⁹Zr-DFO-trastuzumab show residual uptake in the bone ($4.79 \pm 0.65\%$ ID/g and $6.86 \pm 3.02\%$ ID/g at 72 and 120 h, respectively). This bone uptake was confirmed by immunoPET, and images of ⁸⁹Zr-DFO-trastuzumab at 120 h displayed low liver uptake but slightly higher activity in the joints of the hind legs. It is plausible that a slow rate of intratumoral metabolism of ⁸⁹Zr-DFO-trastuzumab leads to the transmetalation of ⁸⁹Zr⁴⁺ ions to a species which is either excreted or sequestered in bone. However, our stability studies and biodistribution data, along with previous reported investigations on other ⁸⁹Zr-DFO-labeled antibodies suggest that metabolism is very limited. [44–46] Full metabolism studies are beyond the scope of this work but further investigations on the fate of ⁸⁹Zr-DFO-trastuzumab *in vivo* are underway.

The studies reported here are consistent with previous investigations and confirm that ⁸⁹Zr is a suitable radionuclide for labeling full, intact antibodies (~150 kDa). [30] The favorable chemistry and image characteristics mean that ⁸⁹Zr has the potential to solve problems associated with, for example, non-optimal half-life (⁶⁴Cu, ⁸⁶Y), high uptake in background tissue (⁶⁴Cu, ⁶⁸Ga, ¹²⁴I), low *in vivo* stability (¹²⁴I; particularly with internalizing antibody-antigen constructs) and poor dosimetry (⁸⁶Y). Furthermore, these studies demonstrate that immunoPET with ⁸⁹Zr-labeled mAbs can be used for both localizing tumors and measuring the long-term effects (>5 days) of drug treatment from a single radiotracer injection. Such measurements cannot be achieved by using previous ⁶⁴Cu-, ⁸⁶Y-, ^{99m}Tc-, and ¹²⁴I-radiolabeled trastuzumab constructs. Along with ¹⁸F-labeled trastuzumab affibodies [29], ⁸⁹Zr-DFO-trastuzumab represents one of the most promising radiotracers for non-invasive immunoPET measurements of HER2/*neu* expression *in vivo*. These studies also showed that, unlike most tyrosine-kinase inhibitors, PU-H71 displays an extended pharmacodynamic profile for Hsp90 inhibition at time points >24 h, and this window of activity is ideal for immunoPET imaging with radioimmunoconjugates such as ⁸⁹Zr-DFO-trastuzumab. As the pharmacodynamic change in HER2/*neu* expression levels is indicative of the potential anti-tumor effects of PU-H71, ⁸⁹Zr-DFO-trastuzumab may also be used to further the clinical development of this, and related Hsp90

inhibitors, by evaluating the dose delivered to the tumor and quantifying the magnitude of the therapeutic response. These immunoPET studies demonstrate that ⁸⁹Zr-DFO-trastuzumab has the potential to be used in the clinic as a specific radiotracer for measuring the long-term effects of treatment with Hsp90 inhibitors.

In conclusion, ⁸⁹Zr-DFO-trastuzumab has been prepared with high radiochemical purity and specific-activity using methods adapted from the literature. The immunoconjugate was found to be stable with respect to loss of the radiolabel *in vitro* and immunoreactivity assays demonstrated that conjugation, radiolabeling and purification chemistries do not compromise the binding affinity or specificity for the HER2/*neu* antigen. Biodistribution and immunoPET experiments indicated that ⁸⁹Zr-DFO-trastuzumab shows excellent potential as a radiotracer for specific non-invasive delineation of HER2/*neu* positive breast tumors *in vivo*. Furthermore, unlike other trastuzumab constructs radiolabeled with shorter-lived nuclides, ⁸⁹Zr-DFO-trastuzumab may be used to measure the long-term pharmacodynamic effects and potentially patient response to treatment using Hsp90 inhibitors including PU-H71. Work towards the clinical translation of ⁸⁹Zr-DFO-trastuzumab and other ⁸⁹Zr-labeled mAbs is underway.

Supporting Information

Text S1 Supplementary Materials and Methods.

Found at: doi:10.1371/journal.pone.0008859.s001 (0.07 MB DOC)

Figure S1 Typical elution profiles observed by using PD-10 size-exclusion chromatography for the purification of ⁸⁹Zr-DFO-trastuzumab from small molecule (<30 kDa) ⁸⁹Zr-radiolabeled impurities and unreacted [⁸⁹Zr]Zr-oxalate (complexed as [⁸⁹Zr]Zr-DTPA). Species with molecular weights >30 kDa elute in the first <2.0 mL of solvent. The two peaks for crude and purified ⁸⁹Zr-DFO-trastuzumab have the same retention time within the full-width half-maximum (FWHM). Found at: doi:10.1371/journal.pone.0008859.s002 (0.14 MB TIF)

Figure S2 (A) Competitive inhibition (blocking) studies. (B) Cellular association with MDA-MB-468 (HER2/*neu*-ve) cells. Found at: doi:10.1371/journal.pone.0008859.s003 (0.25 MB TIF)

Figure S3 Chemical structure of PU-H71 Found at: doi:10.1371/journal.pone.0008859.s004 (0.05 MB TIF)

Figure S4 Plot of the total normalized, average number of coincident counts recorded via immunoPET imaging of BT-474 tumor-bearing mice ($n=4$) versus time/h. Exponential decay regression analysis has been used to calculate the effective lifetime (τ_{eff}/h) and decay constant ($\lambda_{\text{eff}}/h^{-1}$) from which the estimated observed and biological half-lives ($t_{1/2,\text{eff}}$ and $t_{1/2,\text{bio}}$) have been calculated.

Found at: doi:10.1371/journal.pone.0008859.s005 (0.13 MB TIF)

Figure S5 Plot of the total normalized, average number of coincident counts recorded via immunoPET imaging of MDA-MB-468 tumor-bearing mice ($n=4$) versus time/h. Exponential decay regression analysis has been used to calculate the effective lifetime (τ_{eff}/h) and decay constant ($\lambda_{\text{eff}}/h^{-1}$) from which the estimated observed and biological half-lives ($t_{1/2,\text{eff}}$ and $t_{1/2,\text{bio}}$) have been calculated.

Found at: doi:10.1371/journal.pone.0008859.s006 (0.13 MB TIF)

Table S1 Biodistribution data of ⁸⁹Zr-DFO-trastuzumab versus time/h, administered by i.v. tail-vein injection to female, athymic nu/nu mice bearing s.c. BT-474 tumors (90–150 mm³).^a

Found at: doi:10.1371/journal.pone.0008859.s007 (0.11 MB DOC)

Table S2 A comparison of the difference between mean BT-474 tumor uptake values observed in the biodistribution studies in control (vehicle-treated) and PU-H71 treated mice.

Found at: doi:10.1371/journal.pone.0008859.s008 (0.04 MB DOC)

Table S3 Tumor-to-muscle (T/M) ratios have been calculated from volume-of-interest (VOI) analysis of immunoPET images

recorded in dual tumor-bearing (BT-474 and MDA-MB-468) female, athymic nu/nu mice between 1–120 h post-i.v. administration of ⁸⁹Zr-DFO-trastuzumab. The data presented are ratios of mean and maximum (%ID/g) values. Errors associated with VOI activity measurements are large and are strongly dependent on the number and definition of each ROI used in the determination of the VOI. As a consequence of the large errors associated with VOI analysis, and the further exaggeration that ensues from the calculation of ratios, errors associated with the calculated ratios are large, difficult to define and have been omitted to avoid misrepresentation of the data.

Found at: doi:10.1371/journal.pone.0008859.s009 (0.05 MB DOC)

Table S4 Summary of the calculated effective and biological half-lives

Found at: doi:10.1371/journal.pone.0008859.s010 (0.04 MB DOC)

Acknowledgments

We thank Drs. NagaVaraKishore Pillarsetty, Peter M. Smith-Jones and Pat Zanzonico for informative discussions, Thomas Ku for advice with *in vitro* assays and Bradley Beattie for assistance with the PET imaging. We also thank the staff of the Radiochemistry/Cyclotron Core at MSKCC.

Author Contributions

Conceived and designed the experiments: JPH ECL GC JSL. Performed the experiments: JPH ECL VD VAL TT DZ. Analyzed the data: JPH ECL VD VAL GC JSL. Contributed reagents/materials/analysis tools: JPH TT DZ GC. Wrote the paper: JPH GC JSL.

References

- Wu AM, Senter PD (2005) Arming antibodies: prospects and challenges for immunoconjugates. *Nature Biotech* 23: 1137–1146.
- Wu AM (2009) Antibodies and antimatter: The resurgence of immuno-PET. *J Nucl Med* 50: 2–5.
- Boswell CA, Brechbiel MW (2007) Development of radioimmunotherapeutic and diagnostic antibodies: an inside-out view. *Nucl Med Biol* 34: 757–778.
- Nayak TK, Brechbiel MW (2009) Radioimmunimaging with longer-lived positron-emitting radionuclides: potentials and challenges. *Bioconjugate Chem* 20: 825–841.
- Wu AM, Olafsen T (2008) Antibodies for molecular imaging of cancer. *Cancer J* 14: 191–197.
- Hanahan D, Weinberg RA (2000) The hallmarks of cancer. *Cell* 100: 57–70.
- Baselga J, Swain SM (2009) Novel anticancer targets: revisiting ERBB2 and discovering ERBB3. *Nature Rev Cancer* 9: 463–475.
- Yarden Y, Sliwkowski MX (2001) Untangling the ErbB signalling network. *Nature Rev Mol Cell Biol* 2: 127–137.
- Citri A, Yarden Y (2006) EGF-ERBB signalling: towards the systems level. *Nature Rev Mol Cell Biol* 7: 505–516.
- Hynes NE, MacDonald G (2009) ErbB receptors and signaling pathways in cancer. *Curr Opin Cell Biol* 21: 177–184.
- Hynes NE, Lane HA (2005) ERBB Receptors and cancer: the complexity of targeted inhibitors. *Nature Rev Cancer* 5: 580.
- Baselga J (2006) Targeting Tyrosine Kinases in Cancer: The Second Wave. *Science* 312: 1175–1178.
- Beliakoff J, Whitesell L (2004) Hsp90: an emerging target for breast cancer therapy. *Anti-Cancer Drugs* 15: 651–662.
- Mendelsohn J, Baselga J (2006) Epidermal growth factor receptor targeting in cancer. *Semin Oncol* 33: 369–385.
- Solit DB, Chiosis G (2008) Development and application of Hsp90 inhibitors. *Drug Discovery Today* 13: 38–43.
- Mendelsohn J, Baselga J (2003) Status of epidermal growth factor receptor antagonists in the biology and treatment of cancer. *J Clin Oncol* 21: 2787–2799.
- Citri A, Kochupurakkal BS, Yarden Y (2004) The Achilles heel of ErbB-2/HER2: Regulation by the Hsp90 chaperone machine and potential for pharmacological intervention. *Cell Cycle* 3: 51–60.
- Taldone T, Sun W, Chiosis G (2009) Discovery and development of heat shock protein 90 inhibitors. *Bioorg Med Chem* 17: 2225–2235.
- Niu G, Li Z, Cao Q, Chen X (2009) Monitoring therapeutic response of human ovarian cancer with 17-DMAG by noninvasive PET imaging with ⁶⁴Cu-DOTA-trastuzumab. *Eur J Nucl Med Mol Imaging*.
- Smith-Jones PM, Solit DB, Akhurst T, Afroz F, Rosen N, et al. (2004) Imaging the pharmacodynamics of HER2 degradation in response to Hsp90 inhibitors. *Nature Biotechnol* 22: 701–706.
- Smith-Jones PM, Solit D, Afroz F, Rosen N, Larson SM (2006) Early tumor response to Hsp90 therapy using HER2 PET: comparison with ¹⁸F-FDG PET. *J Nucl Med* 47: 793–796.
- Costantini DL, Bateman K, McLarty K, Vallis KA, Reilly RM (2008) Trastuzumab-resistant breast cancer cells remain sensitive to the Auger electron-emitting radiotherapeutic agent ¹¹¹In-NLS-trastuzumab and are radiosensitized by methotrexate. *J Nucl Med* 49: 1498–1505.
- Reilly RM, Chen P, Wang J, Scollard D, Cameron R, et al. (2006) Preclinical pharmacokinetic, biodistribution, toxicology, and dosimetry studies of ¹¹¹In-DTPA-human epidermal growth factor: an auger electron-emitting radiotherapeutic agent for epidermal growth factor receptor-positive breast cancer. *J Nucl Med* 47: 1023–1031.
- Tang Y, Wang J, Scollard DA, Mondal H, Holloway C, et al. (2005) Imaging of HER2/neu-positive BT-474 human breast cancer xenografts in athymic mice using ¹¹¹In-trastuzumab (Herceptin) Fab fragments. *Nucl Med Biol* 32: 51–58.
- Garmestani K, Milenic DE, Plascjak PS, Brechbiel MW (2002) A new and convenient method for purification of ⁸⁶Y using a Sr(II) selective resin and comparison of biodistribution of ⁸⁶Y and ¹¹¹In labeled Herceptin? *Nucl Med Biol* 29: 599–606.
- Palm S, Enmon RM Jr, Matei C, Kolbert KS, Xu S, et al. (2003) Pharmacokinetics and biodistribution of ⁸⁶Y-trastuzumab for ⁹⁰Y dosimetry in an ovarian carcinoma model: Correlative microPET and MRI. *J Nucl Med* 44: 1148–1155.
- Perik PJ, Lub-De Hooge MN, Gietema JA, van der Graaf WTA, de Korte MA, et al. (2006) Indium-111-labeled trastuzumab scintigraphy in patients with human epidermal growth factor receptor 2-positive metastatic breast cancer. *J Clin Oncol* 24: 2276–2282.
- Orlova A, Wallberg H, Stone-Elander S, Tolmachev V (2009) On the selection of a tracer for PET imaging of HER2-expressing tumors: Direct comparison of a ¹²⁴I-labeled affibody molecule and trastuzumab in murine xenograft model. *J Nucl Med* 50: 417–425.
- Kramer-Marek G, Kiesewetter DO, Capala J (2009) Changes in HER2 expression in breast cancer xenografts after therapy can be quantified using PET and ¹⁸F-labeled affibody molecules. *J Nucl Med* 50: 1131–1139.
- Dijkers ECF, Kosterink JGW, Rademaker AP, Perk LR, van Dongen GAMS, et al. (2009) Development and characterization of clinical-grade ⁸⁹Zr-trastuzumab for HER2/neu immunoPET imaging. *J Nucl Med* 50: 974–981.

31. Meijs WE, Herscheid JDM, Haisma HJ, Pinedo HM (1992) Evaluation of desferal as a bifunctional chelating agent for labeling antibodies with Zr-89. *Appl Radiat Isot* 43: 1443–1447.
32. Meijs WE, Haisma HJ, Van der Schors R, Wijbrandts R, Van den Oever K, et al. (1996) A facile method for the labeling of proteins with Zirconium Isotopes. *Nucl Med Biol* 23: 439–448.
33. Meijs WE, Haisma HJ, Kloek RP, van Gog FB, Kievit E, et al. (1997) Zirconium-labeled monoclonal antibodies and their distribution in tumor-bearing nude mice. *J Nucl Med* 38: 112–118.
34. Verel I, Visser Gerard WM, van Dongen Guus A (2005) The promise of immuno-PET in radioimmunotherapy. *J Nucl Med* 46 Suppl 1: 164S–171S.
35. Verel I, Visser GWM, Boellaard R, Boerman O, Van Eerd J, et al. (2003) Quantitative ⁸⁹Zr immuno-PET for in vivo scouting of ⁹⁰Y-labeled monoclonal antibodies in Xenograft-bearing nude mice. *J Nucl Med* 44: 1663–1670.
36. Verel I, Visser GWM, Boellaard R, Stigter-van Walsum M, Snow GB, et al. (2003) ⁸⁹Zr immuno-PET: Comprehensive Procedures for the production of ⁸⁹Zr-labeled monoclonal antibodies. *J Nucl Med* 44: 1271–1281.
37. Verel I, Visser GWM, Boerman O, Van Eerd J, Finn R, et al. (2003) Long-lived positron emitters Zirconium-89 and Iodine-124 for scouting of therapeutic radioimmunoconjugates with PET. *Cancer Biotherapy and Radiopharmaceuticals* 18: 655–661.
38. Verel I, Visser GWM, Vosjan MJWD, Finn R, Boellaard R, et al. (2004) High-quality 124I-labelled monoclonal antibodies for use as PET scouting agents prior to 131I-radioimmunotherapy. *Eur J Nucl Med Mol Imaging* 31: 1645–1652.
39. Perk LR, Visser GWM, Vosjan MJWD, Stigter-van Walsum M, Tjink BM, et al. (2005) ⁸⁹Zr as a PET surrogate radioisotope for scouting biodistribution of the therapeutic radiometals ⁹⁰Y and ¹⁷⁷Lu in tumor-bearing nude mice after coupling to the internalizing antibody Cetuximab. *J Nucl Med* 46: 1898–1906.
40. Perk LR, Stigter-van Walsum M, Visser GWM, Kloet RW, Vosjan MJWD, et al. (2008) Quantitative PET imaging of Met-expressing human cancer xenografts with ⁸⁹Zr-labelled monoclonal antibody DN30. *Eur J Nucl Med Mol Imaging* 35: 1857–1867.
41. Perk LR, Visser GWM, Budde M, Vosjan MJWD, Jurek P, et al. (2008) Facile radiolabeling of monoclonal antibodies and other proteins with zirconium-89 or gallium-68 for PET imaging using p-isothiocyanatobenzyl-desferrioxamine. *Nature Protocols*.
42. Brouwers A, Verel I, Van Eerd J, Visser G, Steffens M, et al. (2004) PET Radioimmunosciintigraphy of renal cell cancer using ⁸⁹Zr-labeled cG250 monoclonal antibody in nude rats. *Cancer Biotherapy and Radiopharmaceuticals* 19: 155–163.
43. Aerts HJWL, Dubois L, Perk L, Vermaelen P, van Dongen GAMS, et al. (2009) Disparity between in vivo EGFR expression and ⁸⁹Zr-labeled cetuximab uptake assessed with PET. *J Nucl Med* 50: 123–131.
44. Perk LR, Visser OJ, Stigter-van Walsum M, Vosjan MJWD, Visser GWM, et al. (2006) Preparation and evaluation of ⁸⁹Zr-Zevalin for monitoring of ⁹⁰Y-Zevalin biodistribution with positron emission tomography. *Eur J Nucl Med Mol Imaging* 33: 1337–1345.
45. Börjesson PKE, Jauw YWS, Boellaard R, de Bree R, Comans EFI, et al. (2006) Performance of immuno-Positron Emission Tomography with Zirconium-89-labeled chimeric monoclonal antibody U36 in the detection of lymph node metastases in head and neck cancer patients. *Clin Cancer Res* 12: 2133–2140.
46. Borjesson PKE, Jauw YWS, de Bree R, Roos JC, Castelijn JA, et al. (2009) Radiation dosimetry of ⁸⁹Zr-labeled chimeric monoclonal antibody U36 as used for immuno-PET in head and neck cancer patients. *J Nucl Med* 50: 1828–1836.
47. Holland JP, Sheh Y, Lewis JS (2009) Standardized methods for the production of high specific-activity zirconium-89. *Nucl Med Biol* 36: 729–739.
48. Caldas-Lopes E, Cerchietti L, Ahn JH, Clement CC, Robles AI, et al. (2009) Hsp90 inhibitor PU-H71, a multimodal inhibitor of malignancy, induces complete responses in triple-negative breast cancer models. *Proc Natl Acad Sci* 106: 8368–8373, S8368/8361–S8368/8314.
49. Zanzonico P (2009) Routine quality control of clinical nuclear medicine instrumentation: a brief review. *J Nucl Med* 49: 1114–1131.
50. Meijs WE, Herscheid JDM, Haisma HJ, Wijbrandts R, van Langevelde F, et al. (1994) Production of highly pure no-carrier added ⁸⁹Zr for the labelling of antibodies with a positron emitter. *Appl Radiat Isot* 45: 1143–1147.
51. Anderson CJ, Connett JM, Schwarz SW, Rocque PA, Guo LW, et al. (1992) Copper-64-labeled antibodies for PET imaging. *J Nucl Med* 33: 1685–1690.
52. Anderson CJ, Schwarz SW, Connett JM, Cutler PD, Guo LW, et al. (1995) Preparation, biodistribution and dosimetry of copper-64-labeled anti-colorectal carcinoma monoclonal antibody fragments 1A3-F(ab')₂. *J Nucl Med* 36: 850–858.
53. Lindmo T, Boven E, Cuttitta F, Fedorko J, Bunn PA Jr (1984) Determination of the immunoreactive fraction of radiolabeled monoclonal antibodies by linear extrapolation to binding at infinite antigen excess. *J Immunol Methods* 72: 77–89.
54. Chandarlapaty S, Sawai A, Ye Q, Scott A, Silinski M, et al. (2008) SNX2112, a Synthetic Heat Shock Protein 90 Inhibitor, Has Potent Antitumor Activity against HER Kinase-Dependent Cancers. *Clin Cancer Res* 14: 240–248.
55. Smith-Jones PM, Solit D, Afroz F, Rosen N, Larson SM (2006) Early tumor response to Hsp90 therapy using HER2 PET: Comparison with ¹⁸F-FDG PET. *J Nucl Med* 47: 793–796.
56. Kim JS, Lee JS, Im KC, Kim SJ, Kim S-Y, et al. (2007) Performance measurement of the microPET Focus 120 scanner. *J Nucl Med* 48: 1527–1535.
57. Taldone T, Gozman A, Maharaj R, Chiosis G (2008) Targeting Hsp90: small-molecule inhibitors and their clinical development. *Curr Opin Pharmacology* 8: 370–374.
58. Fox ME, Szoka FC, Frechet JMJ (2009) Soluble polymer carriers for the treatment of cancer: the importance of molecular architecture. *Acc Chem Res* 42: 1141–1151.
59. Baughman SA, Shak S US Patent 6627196.